High-Velocity Impact Testing and Analysis of Layered Metal-Composite Shields Using Electromagnetic Railguns

Ritabrata Chakraborty[1], Dr. Rishi Verma[2], Shobhna Mishra[3]

[1]BITS Pilani, Rajasthan, India

[2, 3]BARC Vizag, Andhra Pradesh, India

Email: f20220843@pilani.bits-pilani.ac.in

PPSTA-2024

INTRODUCTION

The study investigates the impact resistance of layered composite materials subjected to high-velocity impact, using both experimental and FEM analysis. Materials like SS 304, Al 6061-T6, and GFRP have been strategically layered for optimal energy absorption and protection. Experimental testing with an electromagnetic launcher facility (RAFTAR) at BARC (F), Visakhapatnam, along with simulations based on Johnson-Cook models, provide insights into deformation and failure mechanisms.

Constitutive law:

$$\sigma_y = \left(A + B\bar{\varepsilon}^{p\,n}\right)\left(1 + C ln(\dot{\varepsilon}^*)\right)\left(1 - T^{*m}\right)$$

Failure strain:

$$\varepsilon^f = \left(D_1 + D_2 e^{(D_3\sigma^*)}\right)\left(1 + D_4 ln(\dot{\varepsilon}^*)\right)\left(1 + D_5 T^*\right)$$

where, σ_y = flow stress

A, B, C, n, m = constants

$\bar{\varepsilon}^p$ = effective plastic strain

D_1, D_2, D_3, D_4 = damage constants

$$\dot{\varepsilon}^* = \frac{\dot{\varepsilon}^p}{\dot{\varepsilon}^0} \qquad T^* = \frac{T - T_{room}}{T_{melt} - T_{room}} \qquad \sigma^* = \frac{p}{\sigma_{eff}}$$

Figure: Johnson-Cook Plasticity and Damage Models

METHODOLOGY

Numerical simulations were conducted using a Aluminum 7075-T6 projectile (8 gm) at velocities of 1000 m/s and 472 m/s for 0.0001 and 0.0002 seconds, respectively. The projectile, modeled with 25 hexahedral elements along its front edge and a hex-dominant mesh, impacted GFRP (8 mm), AL 6061-T6 (1 mm and 2 mm), and SS 304 (1 mm and 2 mm) plates. Plates were fixed at the edges with bonded contact, and mesh sizes ranged from 2 mm to 0.5 mm for stress and deformation capture. Erosion controls retained the inertia of failed elements. Z-direction velocity, deformation, and stress-strain responses were analyzed, focusing on normal, shear, and principal stresses at key points.

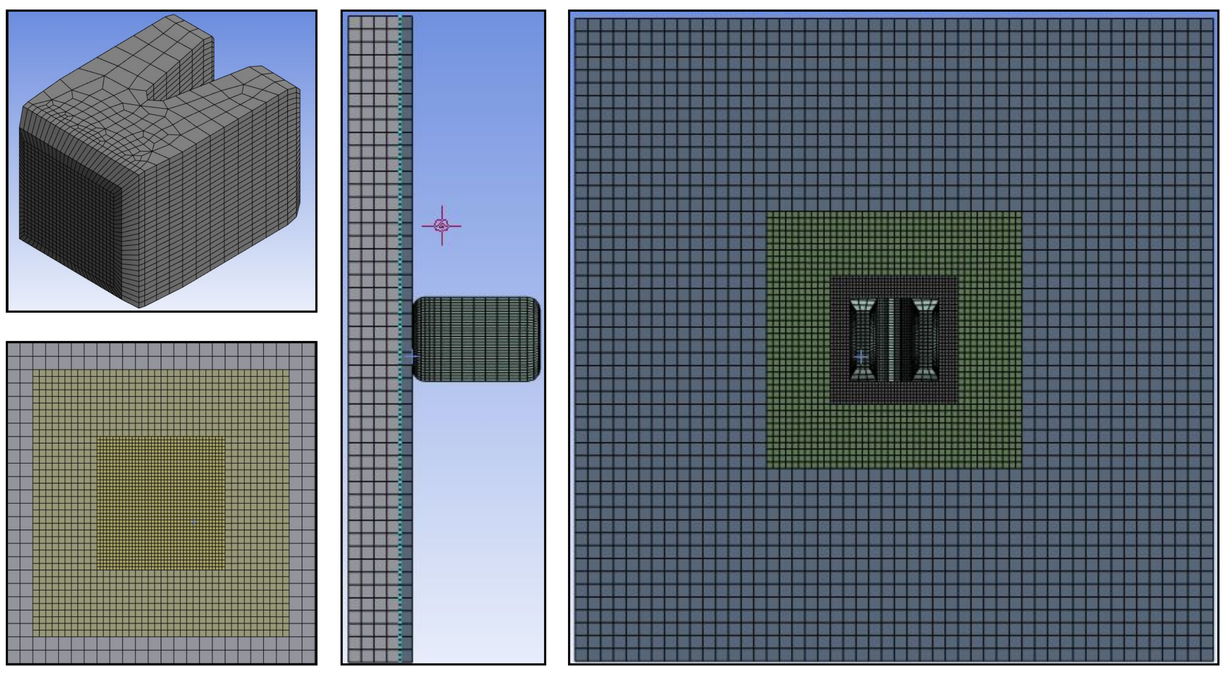

Figure: (Top Left) Projectile Mesh Setup, (Bottom Left) Plate Mesh Setup, (Middle) Side View of Simulation Setup, and (Right View) Front View of Simulation Setup

RESULTS AND DISCUSSION

The simulations showed that a 4mm thick SS (304) effectively stopped the projectile at 1000 m/s. The SS (3mm) and AL (6061-T6, 2mm) composite emerged as the best lighter alternative, offering similar performance. The petalling effect was observed only in SS, while GFRP and AL showed delamination and plastic deformation, respectively, without petalling. This composite effectively balances reduced weight and impact resistance, suggesting it as a viable option for lightweight protection. Further research could focus on optimizing this composite or exploring other materials.

Material	Thickness in mm	Plate Condition	Plate Total Energy in J	Projectile Condition	Projectile Velocity (Z) in m/s	Projectile Kinetic Energy in J
SS	4	Cracked; Not Punctured	2181	Broken; Highly Deformed	~ -15	108.65
SS	3	Punctured	1820.5	Broken; Highly Deformed	~ 335	529.09
GFRP	8	Punctured	1094.5	Intact; Slightly Deformed	~ 680	1992.1

Table 1: Single Material; Velocity: 1000 m/s

0 - 1 mm	1 - 2 mm	2 - 3 mm	3 - 4 mm	4 - 5 mm	Plate Condition	Plate Total Energy in J	Projectile Condition	Projectile Velocity (Z) in m/s	Projectile Kinetic Energy in J
SS	AL	SS	AL	SS	Punctured	1417.4	Intact; Moderately Deformed	~ 480	1025.2
SS			AL		Punctured	1977.7	Broken; Highly Deformed	~ 35	140.63
AL	SS	AL	SS	AL	Punctured	1279.5	Broken; Moderately Deformed	485	965.47

Table 2: Composites with AL - SS (Thickness: 1mm); Velocity: 1000 m/s

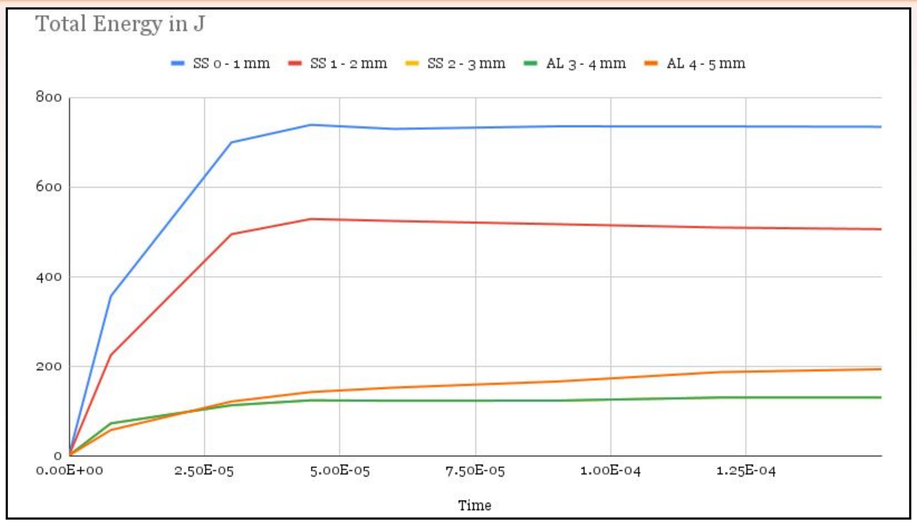

Figure 3: Graph of Total Energy of SS (3mm) - AL (2mm) Composite Plate

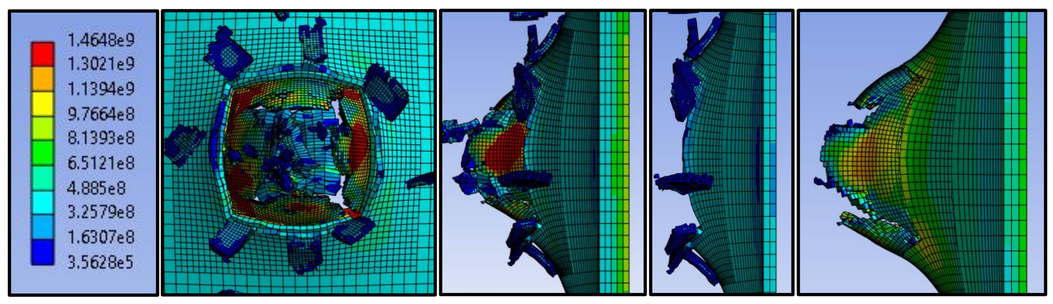

Figure 4: (Left to Right) Scale for Equivalent Stress (in Pa), Front View of Composite Plate (SS - 3mm, AL - 2mm), Side View of Composite Plate (SS - 3mm, AL - 2mm), Side View of AL Plate (2 mm), Side View of SS Plate (3mm) displaying Petalling Effect

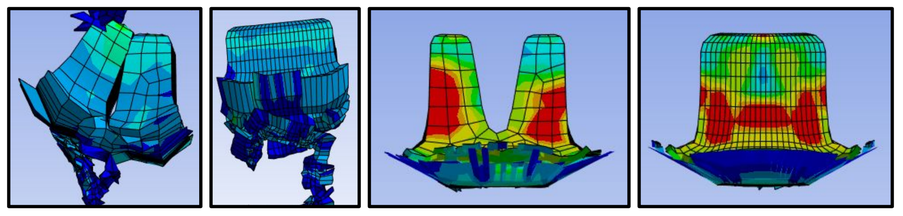

Figure 5: Equivalent Stress (in Pa): (Left to Right) Top View of Projectile After Impact, Side View of Projectile After Impact, Top View of Projectile During Impact, Side View of Projectile During Impact

Materials		Plate Condition	Plate Total Energy in J	Projectile Condition	Projectile Velocity (Z) in m/s	Projectile Velocity (Z) in m/s
SS	GRPF	Punctured	1491.7	Broken; Moderately Deformed	~ 390	689.49
AL	GRPF	Punctured	1197	Intact; Slightly Deformed	~ 615	1610.4
GRPF	SS	Punctured	1508.8	Intact; Slightly Deformed	~ 415	726.82

Table 3: GRPF (Transverse Load) - AL - SS (Thickness: 2mm; GRPF Thickness: 8mm); Velocity: 1000 m/s

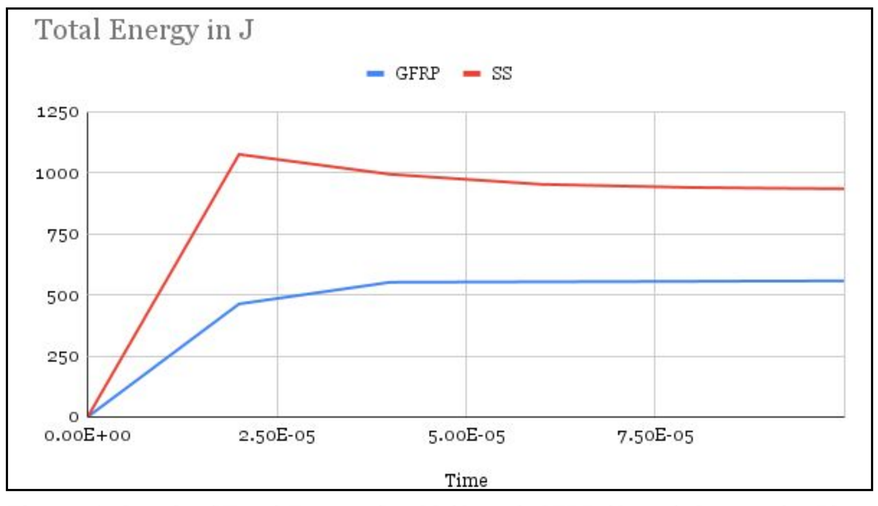

Figure 6: Graph of Total Energy for SS (2mm)-GFRP (8mm) Composite Plate

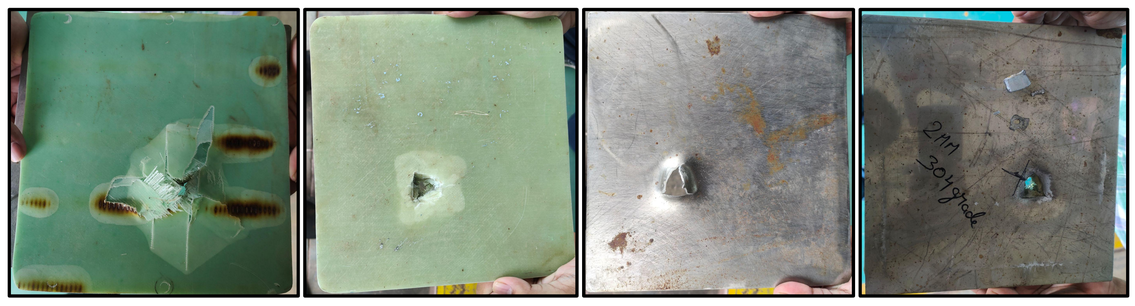

Figure 7: Plate Condition after Impact for SS(2mm) - GFRP (8mm) Composite: (Left to Right) GFRP (8mm) Back and Impact Side, SS 304 (2mm) Back and Impact Side

CONCLUSION

The analysis identifies critical factors affecting projectile deformation and fracture, focusing on AL 7075-T6, AL 6061-T6, SS 304, and GFRP under ballistic impact conditions. AL 7075-T6 shows increased susceptibility to embrittlement from microsegregation and demonstrates distinct brittle-to-ductile and ductile-to-brittle transitions, influenced by thermal softening and work hardening. The C-shaped projectile heightens stress concentration, leading to premature failure.

For SS 316L and SS 304, ballistic impact behavior varies with projectile nose shape, exhibiting different failure modes: shear plugging for blunt projectiles and ductile hole enlargement for ogival projectiles. Numerical simulations indicate that Lode-dependent fracture criteria (MMC) offer better predictions than Lode-independent criteria (MJC). However, both struggle with blunt projectiles due to the exclusion of strain-induced martensitic transformation (SIMT), suggesting a need for refined criteria that incorporate SIMT effects for improved ballistic impact predictions.